The Isomerization of Dinitrogen Tetroxide: $O_2N-NO_2 \rightarrow ONO-NO_2$

André S. Pimentel,*,†,‡ Francisco C. A. Lima,‡ and Albérico B. F. da Silva‡

Departamento de Química, Pontifícia Universidade Católica do Rio de Janeiro, Rua Marquês de São Vicente 225, Gávea, 22453-900 Rio de Janeiro, RJ Brazil, and Instituto de Química de São Carlos, Universidade de São Paulo, Av. Trabalhador São Carlense, 400 C.P 780 São Carlos, SP, Brazil 13566-590

Received: November 23, 2006; In Final Form: February 16, 2007

The N_2O_4 isomerization in gas phase has an energy barrier of 31 kcal mol^{-1} at 298 K. This energy barrier may be reduced due to the interaction of the N_2O_4 isomers with water or nitric acid clusters adsorbed on surfaces. The Gibbs free energy barrier for this reaction in water medium is estimated to be reduced to 21.1 kcal mol^{-1} by using the ab initio calculations and the polarizable continuum model (PCM). By using the transition state theory (TST), this model estimates that the N_2O_4 isomerization may be as fast as 2.0×10^{-3} s^{-1} in aqueous phase at room temperature, which confirms the Finlayson-Pitts model for the heterogeneous hydrolysis of NO_2 on surfaces. The activation energy of the N_2O_4 isomerization is about 21 kcal mol^{-1}. The rate coefficient for this reaction is considerably fast, 1.2×10^{-2} s^{-1}, in aqueous phase at $T = 373$ K.

Introduction

Nitrogen oxides play important roles in the chemistry and physics of wide variety of upper and lower atmospheric systems[1] such as air pollution, acid rain, atmospheric aerosols, and ozone destruction. Their reactions are rather complex, and our knowledge about the chemical mechanisms, or even the structure of those species, is somewhat incomplete. It has been long known that dinitrogen tetroxide (N_2O_4) exists in substantial concentrations in chemical equilibrium at room temperature and atmospheric pressure in the gas phase:

$$NO_2 + NO_2 = N_2O_4 \quad (1)$$

where the N_2O_4 terminology always describes the general formula of dinitrogen tetroxide; its isomers are described as shown in the following. Its more stable conformer has the planar centro-symmetric conformation (O_2N-NO_2) belonging to the D_{2h} point group symmetry.[2−7] The N−N bond length in this compound is relatively longer (1.7561 Å, see Table 1) than that found in hydrazine (N_2H_4),[8−9] and the dissociation energy for this N−N bond is about 13 kcal mol^{-1}.[10−13] The N_2O_4 molecule may also suffer internal rotation (torsion) over the N−N bond with an energy barrier of about 3−8 kcal mol^{-1}.[14] Due to its weak binding, O_2N-NO_2 may undergo isomerization by breaking the N−N bond and linking the oxygen atom to the nitrogen from the other side of the molecule. This isomerization may yield to the asymmetric isomer ($ONO-NO_2$), which has been observed in several studies:[15−25]

$$O_2N-NO_2 \rightarrow ONO-NO_2 \quad (2)$$

The chemical mechanism for the heterogeneous formation of nitrous acid (HNO_2) has been proposed recently by Finlayson-Pitts and collaborators.[26−28] It involves the NO_2 dimerization in gas phase, the O_2N-NO_2 adsorption in a thin-layer of water on surfaces, the O_2N-NO_2 isomerization (Reaction 2) in aqueous phase, the $ONO-NO_2$ ionization to form $NO^+NO_3^-$, and hydrolysis of it to form HNO_2 and HNO_3. The products, HNO_2 and HNO_3, of this chemical mechanism have been detected in many systems.[29−33] However, there are still controversies related to the intermediates, i.e., what does really happen with the N_2O_4 chemistry on surfaces? Is the N_2O_4 isomerization likely to occur at environmental conditions? Several researchers[34−37] have suggested that the presence of the asymmetric isomer leads directly to the formation of the ion pair nitrosonium nitrate, $NO^+NO_3^-$, in thin-film deposits. On the other hand, many studies[38−41] have not detected the asymmetric isomer using high sensitivity spectroscopic methods. In addition, solutions of N_2O_4 in nitric acid show that N_2O_4 is definitely capable to be ionized and forms the ion pair $NO^+NO_3^-$.[42]

The attempt to reveal if the N_2O_4 isomerization plays a role in the heterogeneous hydrolysis of NO_2 proposed in Finlayson-Pitts model[26−28] is the motivation for this study. Furthermore, almost nothing is known about its asymmetric isomer, $ONO-NO_2$, since the experimental structure has not been reported yet and only few theoretical studies have been performed on this molecule so far.[43,44] Due to the lack of information about the asymmetric isomer, this paper will predict the thermodynamical properties of this reasonably new molecule, propose how it should be formed, and its fate on environmental surfaces.

The main aim of this paper is to calculate the reaction path, transition state (TS), and barrier energy for this reaction in gas phase and water medium. It is the first paper to propose the reaction path for the N_2O_4 isomerization, calculate its energy barrier, and estimate its rate coefficient at the temperature range of $T = 273-313$ K. The density functional theory (DFT)[45−47] is applied to this problem to (1) optimize the reactant, product, and transition state; (2) calculate the frequencies of them; (3) calculate the reaction path for the N_2O_4 isomerization; and (4) estimate the rate coefficient using the conventional transition state theory (TST). Another aim is to discuss the possibility and implication for this reaction in atmospheric conditions.

Methodology

The only way to study this complex reaction system is to perform theoretical quantum calculations of the isolated isomer-

* Corresponding author. E-mail: a_pimentel@qui.puc-rio.br.
† Pontifícia Universidade Católica do Rio de Janeiro.
‡ Universidade de São Paulo.

10.1021/jp067805z CCC: $37.00
Published on Web 03/28/2007

TABLE 1: Bond Distances (in Å) and Bond Angle (deg) for the O_2N-NO_2 Molecule, D_{2h}

method	r_e (N−N)	r_e (N−O)	∠ONO
DFT/B3LYP/6-311++G(d,p) (vacuum)	1.810	1.188	134.8
DFT/B3PW91/6-311++G(d,p) (vacuum)	1.783	1.183	134.8
DFT/B3P86/6-311++G(d,p) (vacuum)	1.773	1.183	134.8
DFT/B1B95/6-311++G(d,p) (vacuum)	1.775	1.181	134.9
DFT/B1LYP/6-311++G(d,p) (vacuum)	1.793	1.186	134.7
DFT/MPW1PW91/6-311++G(d,p) (vacuum)	1.757	1.180	134.7
DFT/PBE1PBE/6-311++G(d,p) (vacuum)	1.754	1.180	134.8
DFT/B3LYP/13s8p(2d,1f) (vacuum)	1.803	1.185	134.7
DFT/B3LYP/13s8p(2d,1f) (water)	1.785	1.185	134.5
QCISD/6-311++G(d,p) (vacuum)	1.701	1.190	134.2
CCSD(T)/cc-pVTZ[a] (vacuum)	1.744	1.194	134.8
expt.[b] (ED)[c]	1.776(4)	1.191(4)	134.6(5)
expt.[b] (XD)[d]	1.712(17)	1.189(12)	134.8(15)
expt.[b] (ND)[e]	1.7561(9)	1.1893(5)	134.40(7)
expt.[b] (IRR)[f]	1.756(10)	1.196(5)	133.7(5)

[a] Higher level of calculation performed by Ornellas et al.[67] [b] Uncertainties attached to the last significant digits are given in parentheses. [c] Electron diffraction in gas phase at $T = 294$ K from ref 5. [d] X-ray diffraction in solid state at $T = 25$ K from ref 2. [e] Neutron diffraction at $T = 20$ K from ref 4. [f] Infrared rotationally resolved measurements at $T \approx 50$ K from ref 6.

ization reaction. Our calculations were carried out within the density functional formalism using the Gaussian 03 software.[48] The balance between Hartree−Fock exchange and DFT exchange-correlation in hybrid functionals is believed to be suitable to calculate complex bonding systems.[45−47] We used Becke's three parameter hybrid functionals, which include such mixture of Hartree−Fock exchange with DFT exchange-correlation: (1) B3LYP[49] that uses the nonlocal correlation provided by the LYP expression,[50,51] and VWN[52] functional III for local correlation; (2) B3P86[49] that specifies the same functional with the nonlocal correlation provided by Perdew in 1986;[53] and (3) B3PW91[49] that specifies this functional with the nonlocal correlation provided by Perdew and Wang.[54] We also performed calculations with Becke's one parameter hybrid functionals: (1) B1B95[55] that uses the original Becke's one-parameter hybrid functional as defined in the original paper; (2) B1LYP[55] that uses the LYP correlation functional;[50,51] (3) MPW1PW91[56] that uses modified Perdew and Wang exchange and Perdew and Wang correlation;[54] and (4) PBE1PBE[57,58] that uses the hybrid functional of Perdew, Burke and Ernzerhof with 25% exchange and 75% correlation weighting. The basis sets 6-311++G(d,p), aug-cc-pVTZ, and a set of Gaussian base especially developed with the polynomial Generator Coordinate Hartree−Fock (pGCHF) method[59] were used to perform the calculations in this work. The latter basis sets consist of a 13s8p Gaussian function polarized with 2d and 1f functions. Hereafter we will used the notation 13s8p(2d,1f) for these Gaussian basis sets.

The geometries of the reactant, product, and TS were fully optimized with the aid of analytical gradients using the Berny algorithm with redundant internal coordinates until a stationary point on the potential surface is found. The TS was searched using the synchronous transit-guided Quasi-Newton method (STQN),[61] which requires the reactant, product, and an initial guess for the TS structure as input. The TS was verified by subsequent frequency calculations, which allowed us to determine the imaginary vibrational frequencies related to the reaction path. The remaining *M*-3 points on the path were generated by two successive linear interpolations, first between the reactant and TS and then between the TS and product. The intrinsic reaction coordinate (IRC) was calculated to follow the reaction path of this isomerization, and reassure that the transition structure is really a saddle point of the reaction path. The initial geometry for the TS structure was used as a starting point to follow the path in both directions. Also, the computed force constants in Cartesian coordinates from a frequency calculation of the optimized TS geometry were calculated. The Cartesian force matrix was diagonalized to get the harmonic vibrational frequencies. The imaginary frequency was specified to follow the reaction path of the isomerization. The geometry was optimized at each point along the reaction path so that the segment of the reaction path between any two adjacent points is described by an arc of a circle, and so that the gradients at the end point of the arc are tangent to the path. The procedure is well described in the literature.[48,60]

The polarizable continuum model (PCM)[61] is employed to optimize the reactant, product, and TS structure in a cavity created via a series of overlapping spheres simulating the water solvation. The PCM is based on a description of the solvent as macroscopic continuum medium having suitable properties (dielectric constant, thermal expansion coefficient, etc.). In this procedure, the solute is embedded in a cavity in the dielectric medium, which is defined above. The solute−solvent interactions are described in terms of the reaction field due to the presence of the dielectric medium, which acts as perturbation on the Hamiltonian of the solute through its reaction potential. Then we calculate the free energy of solvation for the reactant, product, and TS in order to evaluate the solvation effect on the N_2O_4 isomerization. This model performs a reaction field calculation using the integral equation formalism (IEF-PCM) model, whose details of the formalism and implementation have been published in the literature.[61]

Frequency calculations on the optimized structures were used to generate the zero-point, thermal, and Gibbs free energy (G) corrections to be added to the potential energy in order to calculate the zero-point-corrected energy, the enthalpy (H), and the Gibbs free energy, respectively. The standard Gibbs free energy in gas phase (G_g) is calculated by adding the potential energy (E_g) to the Gibbs free energy corrections ($G_{c,g}$) calculated at 1 atm:

$$G_g = E_p + G_{c,g}$$

The standard Gibbs free energy in aqueous phase (G_{aq}) is calculated by adding G_g to the standard solvation free energy (G_{solv}), which is determined in the PCM calculations:

$$G_{aq} = G_g + G_{solv}$$

The thermodynamical properties are calculated at 1 atm and temperatures $T = 273$, 283, 293, 298, 303, and 313 K. All energy quantities for the reactants, products, and transition state were corrected for the zero-point energies (ZPE). The temper-

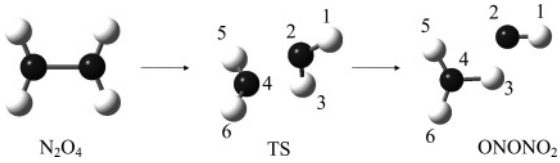

Figure 1. Sketch of the reaction path for the O_2N-NO_2 (D_{2h}) isomerization to the $ONO-NO_2$ (C_s). The transition structure (TS) for the N_2O_4 isomerization and the $ONO-NO_2$ structure are presented with the atom labels to guide the reader. Black atoms are nitrogen and the white ones refer to oxygen.

ature-dependent TST rate coefficient, $k_{TST}(T)$, for the N_2O_4 isomerization is calculated by using the transition state theory,[62] which is given by

$$k(T) = \kappa \frac{k_B T Q^{\#}}{h\ Q_A} \exp\left(\frac{-E_0}{k_B T}\right) = \kappa \frac{k_b T}{hc^0}\left(\frac{RTc^0}{p^0}\right)^{\Delta\nu} \exp\left(\frac{-\Delta G^{\#}_0}{RT}\right) = \kappa k_{TST}(T)$$

The change in the stoichiometry coefficients in isomerization reactions, $\Delta\nu$, is 0, and the concentration c^0 is 1. Thus, the equation above is simplified to

$$k(T) = \kappa \frac{k_B T}{h} \exp\left(\frac{-\Delta G_0}{RT}\right) = \kappa k_{TST}(T)$$

where k_B and h are the Boltzmann and Planck constants, respectively, κ is the transmission coefficient, $Q^{\#}$ is the equilibrium partition function per unit of volume for the transition state, Q_A is the same function for the reactant, and E_0 is the energy of the lowest level of the transition state relative to that of the lowest level of the reactant. The standard Gibbs free energy, $\Delta G^{\#}_0$, in gas or aqueous phase between the TS and reactant can be calculated by standard methods of statistical mechanics to evaluate the equilibrium partition function.

Results and Discussions

The geometry, frequency calculations, and intrinsic reaction coordinates were in fact initially performed using the density functionals: B3LYP, B3P86, B3PW91, B1B95, B1LYP, MPW1PW91, and PBE1PBE. The basis set 6-311++G(d,p) was employed to determine which density functional is more suitable. We also used the basis set aug-cc-pVTZ to calculate some properties as the reader can see below. Then, after choosing the most suitable functional, the 13s8p(2d,1f) basis sets were used to refine the calculations.

O_2N-NO_2. The NO_2 association reaction produces N_2O_4 molecules which has been observed in gas,[63,64] liquid,[20] and solid phases.[17,65] The studies of electron diffraction in gas phase at $T = 294$ K,[5] X-ray[2] and neutron[4] diffractions in solid state at T ≈ 25 K, and infrared rotationally resolved measurements in solid phase at T ≈ 50 K[6] established a D_{2h} structure for the most stable N_2O_4 isomer, O_2N-NO_2. The results of these studies,[2−6,17,20,64−65] our structure calculations performed by density functional theory and QCISD, and a higher level of calculation[67] for the ground state (^1A_g) of the symmetric N_2O_4 are summarized in Table 1. The sketch of the symmetric isomer is shown is shown in Figure 1. The literature shows Hartree−Fock calculations underestimate and second-order Møller-Plesset perturbation theory (MP2) calculations overestimate the N−N bond by as much as 0.2 Å.[4,66] On the other hand, the coupled cluster with singles and double excitations (CCSD) and complete active space self-consistent field (CASSCF) methods offered a reasonable agreement.[67,68] We also found the quadratic configuration interaction calculation including single and double substitutions (QCISD) method with the 6-311++G(d,p) basis set underpredicts the gas-phase experimental structure in almost 0.08 Å. Thus, we preferred to use the DFT method with hybrid functionals, which are less expensive in terms of computational time and give results in excellent agreement with experimental measurements and higher level calculations cited above.

We calculated the N−N bond energy to compare the MP2 and DFT performances. The MP2/6-311++G(d,p) method gave a N−N bond energy of 17.9 kcal mol^{-1}, and the DFT/B3LYP/6-311++G(d,p) methodology resulted in 12.1 kcal mol^{-1}. The experimental values for this N−N bond energy ranges from 13.1 to 13.7 kcal mol^{-1}.[3,11] The energies for this bond calculated with high level of theory are 7.1,[69] 9.6,[70] 10.9,[68] and 12.8[67] kcal mol^{-1}. We also improved this DFT calculation using a large triple-ζ Dunning's correlation consistent basis set augmented with diffuse functions, aug-cc-pVTZ. The DFT/B3LYP method with the Dunning correlation base resulted in 13.2 kcal mol^{-1}, which is within the experimental range for the N−N bond energy. The MP2 method had the largest BSSE error, 4.50 kcal mol^{-1}, while the DFT method had only 1.50 kcal mol^{-1} with 6-311++G(d,p), and 0.36 kcal mol^{-1} with the Dunning correlation basis set. Our results show the DFT method is better than the MP2 and QCISD methods for handling the N_2O_4 geometry calculations. At this point, we already started to suspect that the difficult to describe the N−N bond is a matter of the basis set, instead of the method. Thus, we decided to develop Gaussian basis sets by using the pGCHF method,[59] and especially optimized in the DFT/B3LYP environment, with the aim of observing if we could improve the calculations performed in this study.

There are 12 vibrational modes for the symmetric isomer; 8 modes are inactive, and only four modes are active, which are due to the high degree of symmetry found in this molecule. The vibration modes are represented in Table 2 in order of increasing wavenumber, ω_n: torsion mode (a_u), NO_2 symmetric rocking (b_{2u}), N−N stretching (a_g), NO_2 asymmetric wagging (b_{2g}), NO_2 asymmetric rocking (b_{1g}), NO_2 asymmetric bending (b_{3u}), NO_2 symmetric wagging (b_{1u}), NO_2 symmetric bending (a_g), NO_2 symmetric stretching (b_{3u}), NO_2 symmetric stretching (a_g), NO_2 asymmetric stretching (b_{1g}), and NO_2 asymmetric stretching (b_{2u}).

The experimental[71] and theoretical vibrational frequencies of O_2N-NO_2 are given in Table 2. The theoretical vibration frequencies have a fair agreement with the experimental vibration frequencies. The B3LYP functional gives the best reproduction of experimental vibration frequencies over any used functionals. In fact, the zero-point vibrational energy (ZPVE, in kcal mol^{-1}) calculated by this functional has also better agreement with its experimental value, 14.1 kcal mol^{-1}.[71] On the other hand, Table 1 shows that the geometry calculated by the B3LYP functional does not agree as well as those calculated with the other functionals used in this study. However, it is important to note that the calculations are performed in vacuum and should give better agreements with the geometry determined by electron diffraction in gas phase at $T = 294$ K.[5] The difference between the DFT/ B3LYP calculations and the experimental gas-phase structure is only 0.03 Å.

The PCM model was employed to simulate the water solvation in this complex system. The DFT/B3LYP/13s8p-(2d,1f) methodology was used to describe the N_2O_4 molecule. We observed that the N_2O_4 structure and frequencies are slightly modified by water solvation. Table 1 also presents that the length

TABLE 2: The Experimental and Theoretical Harmonic Vibrational Frequencies (cm^{-1}) for the O_2N-NO_2 Molecule, D_{2h}

method	ω_1 (a_u)	ω_2 (b_{2u})	ω_3 (a_g)	ω_4 (b_{2g})	ω_5 (b_{1g})	ω_6 (b_{3u})	ω_7 (b_{1u})	ω_8 (a_g)	ω_9 (b_{3u})	ω_{10} (a_g)	ω_{11} (b_{1g})	ω_{12} (b_{2u})
DFT/B3LYP/6-311++G(d,p) (vacuum)	83	225	292	436	492	673	762	849	1306	1448	1794	1828
DFT/B3PW91/6-311++G(d,p) (vacuum)	83	236	304	449	508	693	775	859	1336	1474	1844	1878
DFT/B3P86/6-311++G(d,p) (vacuum)	84	239	310	450	512	695	776	861	1339	1475	1848	1882
DFT/B1B95/6-311++G(d,p) (vacuum)	86	256	318	452	512	696	776	861	1345	1483	1859	1894
DFT/B1LYP/6-311++G(d,p) (vacuum)	83	235	301	447	502	687	770	855	1316	1456	1805	1839
DFT/MPW1PW91/6-311++G(d,p) (vacuum)	83	249	319	463	524	711	786	868	1356	1489	1870	1904
DFT/PBE1PBE/6-311++G(d,p) (vacuum)	84	252	322	464	527	714	787	869	1361	1492	1878	1913
DFT/B3LYP/13s8p(2d,1f) (vacuum)	86	224	293	438	494	671	759	850	1302	1446	1779	1815
DFT/B3LYP/13s8p(2d,1f) (water)	109	236	302	450	505	695	724	851	1274	1446	1756	1769
QCISD/6-311++G(d,p) (vacuum)	53	282	352	474	540	684	783	858	1328	1428	1791	1818
expt[71a]	79	254	265	436	484	677	751	806	1261	1382	1724	1757
		265	281	441	498	707	776	826	1294	1413	1777	1818

[a] The experimental frequencies represents the lower and upper limits summarized in the most recent literature.[71] Only one measurement.

TABLE 3: Bond Distances (in Å) and Bond Angle (deg) for the Planar $ONO-NO_2$ Molecule, C_s[a]

parameters	DFT/B3LYP/6-311++G(d,p) (vacuum)	DFT/B3LYP/13s8p(2d,1f) (vacuum)	DFT/B3LYP/13s8p(2d,1f) (water)	QCISD/6-311++G(d,p) (vacuum)
r_e (N4−O5)	1.205	1.201	1.219	1.203
r_e (N4−O3)	1.421	1.421	1.331	1.417
r_e (O3−N2)	1.638	1.620	1.861	1.562
r_e (N2−O1)	1.130	1.129	1.095	1.144
∠O5−N4−O6	130.0	130.1	125.6	130.3
∠O5−N4−O3	117.3	117.4	119.1	113.2
∠N2−O3− N4	111.7	111.3	113.9	108.9
∠O1−N2−O3	107.5	107.6	106.3	107.8

[a] The atom labels are presented to guide the reader in Figure 1.

of the N−N bond decreases in almost 0.02 Å as compared with that calculated in vacuum. That means the water solvation stabilizes the weakly bonded N_2O_4 structure. The vibrational frequencies of the solvated N_2O_4 structure are slightly shifted, but there is not a particular shift direction as it can be seen in Table 2.

A more detailed study of these frequency calculations shows that the anharmonic effects are substantial as suggested by Wesolowski et al.[68] We also observed the anharmonic corrections in the vibrational frequencies are substantial for all DFT calculations of vibrational frequencies, except the DFT calculations using the 13s8p(2d,1f) since no anharmonic corrections were necessary when we used these basis sets. Therefore, the anharmonic effects are as important as using a suitable basis sets to achieve better frequency values using density functional theory with this challenging molecule. Several vibrational modes associated with N−N and NO_2 groups are very important, and then affected in the reaction path. Especially for the reaction path studied here, it is important to emphasize that the frequency of these modes have an excellent agreement with the experimental values as shown in Table 2.

It is worth keeping in mind that vibrational frequencies are more difficult to be evaluated than structure; to achieve better results is necessary to use both larger basis sets and more robust correlation methods. The use of density functional theory with the double or triple-ζ Dunning's correlation consistent basis set does give better results in terms of frequency, but much poorer results in structure. Moreover, the computational time of this approach is a limitation to perform more sophisticated calculations for such complex system.

$ONO-NO_2$. The asymmetric N_2O_4 structure has only been observed in condensed phases. The IR[21] and Raman[42] studies for this molecule are consistent with a planar structure, where NO_2 and NO groups are linked through an N−O−N bridge. Since the experimental structure has not been reported yet and only two theoretical study have been performed on this molecule so far,[43,44] it is interesting to see the predicted properties emerging from this study. We suppose that, due the similarity of both isomers in bonding, the density functional theory may also optimize effectively the geometry of the asymmetric isomer and predict its vibrational properties. The results of our structure calculations for the ground state of the C_s asymmetric N_2O_4 are summarized in Table 3. The sketch of the asymmetric isomer is shown in Figure 1. The atoms labels are set to guide reading Table 3. It is important to observe that the water solvation has a substantial effect on the N−O−N bridge.

There are also 12 vibrational modes in this asymmetric molecule; however, the number of active modes is now increased due to the lack of symmetry. Only three modes are inactive, and the remaining 9 vibrational modes are active. The vibration modes are represented in Table 4 in order of increasing wavenumber, ω_n: NO_2 torsion mode (A″), NO torsion mode (A″), NO_2 rocking (A′), O−N(O) stretching (A′), N−O−N bending (A′), O═N−O bending (A′), NO_2 wagging (A″), NO_2 bending (A′), O−NO_2 stretching (A′), NO_2 symmetric stretching (A′), NO_2 asymmetric stretching (A′), and NO stretching (A′).

The experimental[17,20,21,36,72,73] and theoretical vibrational frequencies of $ONO-NO_2$ molecule are given in Table 4. It seems the DFT/B3LYP methodology again describes the $ONO-NO_2$ molecule better than the QCISD method if we consider only the agreement with experimental frequencies. The anharmonic effect is as large as that found for the O_2N-NO_2 molecule. The experimental structure and vibrational frequencies could be largely affected by the environment. Table 4 presents that several vibrational modes related to the N−O−N bridge are affected by water solvation. The $ONO-NO_2$ molecule is ionized in water medium, producing several shifts in its infrared spectrum. The two most characteristics are as follows. The NO stretching at 1929 cm^{-1} is shifted to 2130 cm^{-1} as it ionizes, and this behavior is confirmed by the experiment as the reader can see in Table 4. The opposite occurs with the NO_2 asymmetric stretching at 1700 cm^{-1}, which shifts to 1524 cm^{-1}.

TABLE 4: Theoretical and Experimental Harmonic Vibrational Frequencies (cm^{-1}) for the Planar ONO−NO_2 Molecule (C_s)

method	ω_1 (A″)	ω_2 (A″)	ω_3 (A′)	ω_4 (A′)	ω_5 (A′)	ω_6 (A′)	ω_7 (A″)	ω_8 (A′)	ω_9 (A′)	ω_{10} (A′)	ω_{11} (A′)	ω_{12} (A′)
DFT/B3LYP/6-311++G(d,p) (vacuum)	48	123	208	297	492	640	765	806	934	1324	1705	1952
DFT/B3LYP/13s8p(2d,1f) (vacuum)	46	125	214	305	491	640	769	807	941	1323	1700	1929
DFT/B3LYP/13s8p(2d,1f) (water)	64	99	167	231	502	705	760	806	973	1272	1524	2130
QCISD/6-311++G(d,p) (vacuum)	81	131	245	346	532	670	767	838	971	1361	1728	1877
expt[17,20,21,36,72,73,a]	50	167	221	304	488	641	721	783	900	1251	1601	1828
						647	762	824	905	1290	1742	1861
expt[20,21,36,73,a] for $ON^+NO_3^-$	62	133	173	258	532	678	−	836	1032[b] 1056[b]	1346[b] 1360[b]	1435[b]	2234[b]

[a] The experimental frequencies represents the lower and upper limits summarized in the most recent literature.[73] [b] These features are assigned to be related to the ONO-NO_2 ionization in the literature.[20,21,36,73]

TABLE 5: Energy Comparison in ΔE of the Two Basis Sets for the NO_2, O_2N-NO_2, and ONO−NO_2 Molecules Using the DFT/B3LYP and HF Methodologies

	energy (Hartree)[a]		
methodology	NO_2	O_2N-NO_2	ONO−NO_2
DFT/B3LYP/6-311++G(d,p)	−205.131908	−410.279798	−410.262862
DFT/B3LYP/13s8p(2d,1f)	*−205.167838*	*−410.351260*	*−410.335096*
ΔE^b	0.03593	0.071462	0.072234
	(22.5)	(44.8)	(45.3)
HF/6-311++G(d,p)	−204.082927	−408.132407	−408.143980
HF/13s8p(2d,1f)	*−204.122777*	*−408.212715*	*−408.223617*
ΔE^b	0.03985	0.080308	0.079637
	(25.0)	(50.4)	(50.0)

[a] All the energies took into account the zero-point correction. [b] The energies in parenthesis are in kcal mol^{-1}.

It is important to note that there is great confusion in the experimental data because both species, ONO−NO_2 and $NO^+NO_3^-$, are usually found as a mixture. For instance, the literature[17,20,21,36,72,73] assigns the features 62, 133, 721, 836, 1346, and 2234 cm^{-1} to the $NO^+NO_3^-$. However, it is only clear to observe the shift in the NO stretching and NO_2 asymmetric stretching from our calculations. It is contradictory the assignment of the NO_2 symmetric stretching for the ionized ONO−NO_2. While we found there is a shift to a low wavenumber as the ONO−NO_2 ionizes, experimental observations sometimes present the opposite. In fact, it is necessary to be cautious as reading the literature[17,20,21,36,72,73] and it is worthy to revise them carefully.

Basis Sets Comparison. In general, the geometries, vibrational frequencies, and potential energy surfaces calculated by the two basis sets, i.e., the 6-311++G(d,p) and 13s8p(2d,1f), presented similar results. Table 5 presents the energy comparison for the NO_2, O_2N-NO_2, and ONO−NO_2 molecules calculated with the two basis sets and using the DFT/B3LYP and HF methodologies. From there, one can see that the DFT/B3LYP and HF energies obtained with the 13s8p(2d,1f) basis sets are around 23 kcal mol^{-1} for NO_2, and 45 kcal mol^{-1} for O_2N-NO_2 and ONO−NO_2 lower than those calculated using the 6-311++G(d,p) basis sets.

Reaction Path of the N_2O_4 Isomerization. The DFT/6-311++G(d,p) method located a stationary structure on the potential surface of the N_2O_4 isomerization. The harmonic vibrational frequencies for this prospective planar TS are not presented here; however, we observed that several frequencies are shifted, including those related to the symmetric N−N stretch and NO_2 asymmetric rock. The imaginary vibrational frequency possibly related to the reaction path is calculated to be (850 ± 44)i cm^{-1} by the DFT/6-311++G(d,p) methodology. Another inactive, low imaginary frequency, (165 ± 5)i cm^{-1}, is assigned to be related to the NO_2 group. Although one of the imaginary frequencies pointed toward the reactants and products, the structure is a second-order saddle point, and not a transition state that connects two minima. If we consider it as a real transition state for the N_2O_4 isomerization, the energy barrier of this reaction is unreasonable, (60 ± 2) kcal mol^{-1} as explained later.

Many attempts to find the planar TS structure using the DFT/13s8p(2d,1f) and QCISD/6-311++G(d,p) methodologies have failed. We used (1) a standard optimization to search a TS rather than a local minimum and (2) the STQN method as geometry optimization of a first-order saddle point, even relaxing various limits on maximum and minimum force constants and step sizes enforced by the Berny algorithm. Indeed, we again suspected the 6-311++G(d,p) basis sets applied with several functionals were not good enough to describe this complex potential surface and find the planar TS. Indeed, we found a nonplanar TS structure using the DFT/ B3LYP/13s8p(2d,1f) and the QCISD/6-311++G(d,p) methodologies. Nevertheless, the QCISD/6-311++G(d,p) method again gave an unreasonable energy barrier, 43.3 kcal mol^{-1}. Unfortunately, it was not possible to perform calculations with the QCISD/13s8p(2d,1f) method, which extrapolated the memory limit for our software version.

The imaginary frequency of the true TS found using the DFT/B3LYP/13s8p(2d,1f) is 319i cm^{-1}, which is related to the reaction path as confirmed by the intrinsic reaction coordinate. The sketch of the nonplanar TS is shown in Figure 1, where the atoms labels can be seen to guide reading Table 6. The TS structure is obtained when the N−N weak bond bends and breaks via torsion, affecting mainly the N−N bond and NO_2 group. The D_{2h} symmetry of the reactant is broken to form the TS with C_s symmetry, which has a three-atom interacting site replaced by an N−O−N bridge in the product, ONO−NO_2. The left-hand side N−O bond of this bridge is much stronger and shorter than the right-hand side O−N bond. Table 7 presents the frequencies of the transition state, including its imaginary frequency.

The Gibbs free energy, ΔG, for the N_2O_4 isomerization in gas phase at 298 K calculated by using the DFT/B3LYP/13s8p-(2d,1f) methodology is +9.9 kcal mol^{-1}, which is in fair agreement with that found for "water-free" condensed phase in the literature, +4.8 kcal mol^{-1}.[21] Thus, this reaction is thermo-

TABLE 6: Bond Distances (in Å), and Bond and Dihedral Angles (deg) for the Transition State of the N_2O_4 Isomerization[a]

	nonplanar TS	
parameters	DFT/B3LYP/13s8p(2d,1f) (vacuum)	DFT/B3LYP/13s8p(2d,1f) (water)
r_e (N4−O5)	1.165	1.141
r_e (N4−O3)	1.792	2.223
r_e (O3−N2)	1.351	1.273
r_e (N2−O1)	1.177	1.211
∠O5−N4−O6	139.8	152.4
∠O5−N4−O3	110.1	102.7
∠N2−O3− N4	86.9	74.0
∠O3−N2−O1	125.1	117.6
∠O1−N2−O3−N4	180.0	180.0

[a] The atom labels are presented to guide the reader in Figure 1.

TABLE 7: Harmonic Vibrational Frequencies (cm^{-1}) for the Nonplanar Transition State of the N_2O_4 Isomerization

method	ω_1 (A′)	ω_2 (A″)	ω_3 (A″)	ω_4 (A′)	ω_5 (A′)	ω_6 (A″)	ω_7 (A′)	ω_8 (A′)	ω_9 (A′)	ω_{10} (A′)	ω_{11} (A′)	ω_{12} (A′)
DFT/B3LYP/ 13s8p(2d,1f) (vacuum)	319i	132	164	270	451	579	673	742	922	1363	1703	1928
DFT/B3LYP/ 13s8p(2d,1f) (water)	543i	106	185	229	322	402	471	781	1178	1321	1500	2127

TABLE 8: Temperature-Dependent Gibbs Free Energies, $\Delta G_0^{\#}$ (kcal mol^{-1}), TST Rate Coefficient, k_{TST} (s^{-1}), and the Lifetime (s) for the N_2O_4 Isomerization in Gas Phase and Water Medium at the Temperature Range $T = 273-313$ K

method	T (K)	$\Delta G_0^{\#}$(T) (kcal mol^{-1})	k_{TST}(T) (s^{-1})	τ (s)
DFT/B3LYP/13s8p(2d,1f) (gas phase)	298	31.3	7.0×10^{-11}	1.4×10^{10}
DFT/B3LYP/13s8p(2d,1f) (water)	273	21.18	6.3×10^{-5}	1.6×10^{4}
	283	21.15	2.7×10^{-4}	3.7×10^{3}
	293	21.13	1.1×10^{-3}	945
	298	21.12	2.0×10^{-3}	494
	303	21.10	3.8×10^{-3}	265
	313	21.08	1.2×10^{-2}	80

dynamically unfavorable to occur at these conditions. Furthermore, the Gibbs free energy barrier, $\Delta G_0^{\#}$, for the transition state formation in this reaction is 31.3 kcal mol^{-1} in gas phase at 298 K using the DFT/B3LYP/13s8p(2d,1f) method. This energy barrier yields a rate coefficient of 7.0×10^{-11} s^{-1}, and consequently, a too long lifetime for the N_2O_4 isomerization, about 10^{10} s. In other words, this reaction may be impossible to occur in gas-phase if this energy barrier is true.

The standard solvation free energies, G_{solv}, of the N_2O_4 and ONO−NO_2 molecules at 298 K are, respectively, −4.8 and −13.8 kcal mol^{-1} using the DFT/B3LYP/13s8p(2d,1f) method. As the G_{solv} of the ONO−NO_2 is almost three times that for the N_2O_4 molecule, the ΔG for the N_2O_4 isomerization becomes nearly zero. Considering that the error bars for this kind of calculation may be quite large (10−20%), it is quite possible that this reaction may be spontaneous in water medium. The energetic diagram for the Gibbs free energy of the N_2O_4 isomerization is presented in Figure 2.

The TST rate coefficient, k_{TST}, for the N_2O_4 isomerization at 298 K is estimated to be 7.0×10^{-11} s^{-1} in gas phase. The lifetime for this reaction occurs at these conditions is too long, about 450 years. If we consider the $\Delta G_0^{\#}$ has an error bar of ± 20% (±6.2 kcal mol^{-1}), the upper limit rate coefficient can achieve 2.5×10^{-6} s^{-1} in gas phase and its lifetime is still long, about 5 days. If this is true, we may now believe this reaction does not occur in gas phase at 298 K. On the other hand, the calculated $\Delta G_0^{\#}$ for the N_2O_4 isomerization in water medium is 21.1 kcal mol^{-1} using the DFT/B3LYP/13s8p-(2d,1f) methodology. The k_{TST} of this reaction at 298 K is estimated to be much faster in water medium; 2.0×10^{-3} s^{-1}, considering the calculated $\Delta G_0^{\#}$ for the N_2O_4 isomerization mediated by water solvation. The lifetime for this reaction occurs at these conditions is now short, 494 s. It is not the intention of this investigation to evaluate the transmission coefficient of this reaction using the Kramers Theory.[62] However, it is important to inquire on the estimate of the transmission coefficient for this reaction. It is well-known that the transmission coefficient for S_N2 reactions is estimated to be 0.8.[62] While S_N2 reactions are dependent on the medium and reactant structures, it is reasonable to affirm that the N_2O_4 isomerization should not have any constraint (steric effect and solvent friction) to occur in water medium since it is an unimolecular reaction. Instead, it may be favored by water medium, suggesting the transmission coefficient of this reaction may be closer to 1 than in S_N2 reactions.

Table 8 shows the temperature-dependent rate coefficient for the N_2O_4 isomerization within the temperature range of 273 to

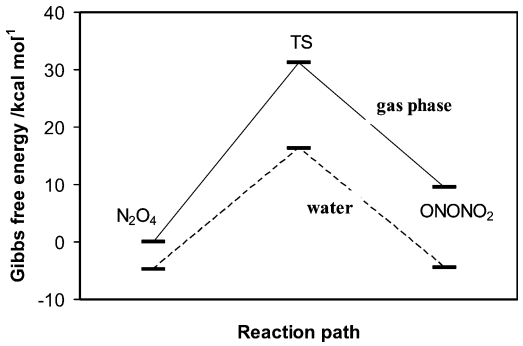

Figure 2. The energetic diagram of the N_2O_4 isomerization in gas phase (straight line, —) and water medium (— — —). The Gibbs free energy, G, is relative to that for the N_2O_4 molecule in gas phase.

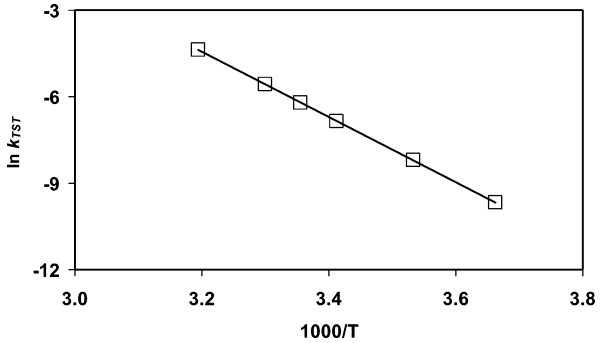

Figure 3. Arrhenius plot for the N_2O_4 isomerization within the temperature range of $T = 273-313$ K.

313 K. The $\Delta G_0^{\#}$ for the N_2O_4 isomerization is not affected by temperature. The Arrhenius plot for the N_2O_4 isomerization is presented in Figure 3, which can be used to calculate the activation energy for this reaction, 21 kcal mol^{-1}.Using this energy barrier, the rate coefficient for this reaction is 1.2×10^{-2} s^{-1} at 313 K, indicating its reaction lifetime may reach only 80 s.

The procedure proposed here in this study is of great importance because it definitely rules out the homogeneous hydrolysis of NO_2 presented in literature.[74] The methodology proposed here overcome many difficulties on working with a system of many atoms and degrees of freedom such as in $N_2O_4 \cdot nH_2O$ investigated in ref 74. It also indicates that TS structure may be clearly stabilized by water molecules, lowering the energy barrier for the N_2O_4 isomerization. The results presented here steps forward to solve an important open problem in Atmospheric Chemistry. Here it is also interesting to pay attention to the fact that the DFT/B3LYP/13s8p(2d,1f) methodology was always the best method to study the N_2O_4 isomerization in gas phase and water solvation.

Atmospheric Implications. The N_2O_4 isomerization in water medium may occur on surfaces with thin layers of water or aqueous aerosols. The observation of the ONO−NO_2 molecule may then be difficult in gas phase since its formation may not occur at this phase. Indeed, our results show this reaction really needs water and/or a nitric acid−water solution, which can be easily found on environment surfaces, i.e., soil, buildings, roads, vegetation, ice, glass, wood, metals, and so on.[25] Unfortunately, the PCM model cannot be applied with a strong ionizing medium, such as nitric acid−water solution, to investigate the heterogeneous hydrolysis of NO_2 on environmental surfaces. This hydrolysis simultaneously forms nitrous acid (HNO_2) and nitric acid (HNO_3) during the reaction. The effect of nitric acid on this reaction may be much stronger than that of water due to their higher strength of hydrogen bonds with the two N_2O_4 isomers, lowering considerably the energy barrier for the N_2O_4 isomerization found here in our study. Thus, the attack of water and HNO_3 on the ONO−NO_2 molecule may have a substantial effect on the Gibbs free energy of this reaction, and consequently, in the HNO_2 formation from the heterogeneous hydrolysis of NO_2. The attack of water and nitric acid on the N−O−N bridge (especially, in the oxygen atom) increases the N−O bond, which may assist the ONO−NO_2 ionization to form the observed $NO^+NO_3^-$ species in the aqueous phase. This is totally reasonable due to the presence of nitric acid in water, a highly ionizing medium. In fact, the literature[25] suggests the presence of highly undissociated HNO_3 hydrates, which may have important catalytic properties for this reaction on environment surfaces. The $NO^+NO_3^-$ species can be hydrolyzed to form HNO_2, which is delivered to the gas phase and photolized to form the important OH radicals in polluted troposphere.

Conclusions

Differently from all the methods, functionals, and basis sets used in this work, the combination DFT/B3LYP/13s8p(2d,1f) was always successful to investigate the N_2O_4 potential energy surface. The Gibbs free energy barrier of the N_2O_4 isomerization in gas phase is 31 kcal mol^{-1}. The PCM model allowed us to evaluate the Gibbs free energy barrier for this reaction in the water medium on environmental surfaces, which may be reduced to about 21 kcal mol^{-1}. This model estimates that the N_2O_4 isomerization may be as fast as 2.0×10^{-3} s^{-1} in aqueous phase at room temperature, confirming the Finlayson-Pitts model for the heterogeneous hydrolysis of NO_2 on surfaces. Using the Arrhenius plot, the energy activation for this reaction is estimated to be about 21 kcal mol^{-1}. The rate coefficient of this reaction may reach 1.2×10^{-2} s^{-1} at 313 K. The interactions of water and HNO_3 with N_2O_4 species may affect the rate of this process, which allows us to address the atmospheric implications of the N_2O_4 isomerization.

Acknowledgment. The authors are grateful to FAPESP, CNPq, and CAPES (Brazilian agencies) for the financial support (04-08227/5). A. S. P. also thanks FAPESP for a research fellowship (05/50722-6).

References and Notes

(1) Finlayson-Pitts, B. J.; Pitts, J. N., Jr. *Chemistry of the Upper and Lower Atmosphere: Theory, Experiments and Application*; Academic Press: New York, 2000.
(2) Cartwright, B. S.; Robertson, J. H. *Chem. Commun.* **1966**, *3*, 82.
(3) Mc Clelland, B. W.; Gunderson, G.; Hedberg, K. *J. Chem. Phys.* **1972**, *56*, 4541.
(4) Kvick, A.; McMullan, R. K.; Newton, M. D. *J. Chem. Phys.* **1982**, *76*, 3754.
(5) Borisenko, K. B.; Kolonits, M.; Rozsondaia, B.; Hargittai, I. *J. Mol. Struct.* **1997**, *121*,413.
(6) Domenech, J. L.; Andrews, A. M.; Belov, S. P.; Fraser, G. T.; Lafferty, W. J. *J. Chem. Phys.* **1994**, *100*, 6993.
(7) Shen, Q.; Hedberg, K. *J. Phys. Chem. A* **1998**, *102*, 6470.
(8) Kohata, K.; Kukuyama, T.; Kuchitsu, K. *J. Phys. Chem.* **1982**, *86*, 602.
(9) Machado, F. B. C.; Roberto-Neto, O. *Chem. Phys. Lett.* **2002**, *352*, 120.
(10) Giauque, W. F.; Kemp, J. D. *J. Chem. Phys.* **1938**, *6*, 40.
(11) Hisatsune, I. C. *J. Phys. Chem.* **1961**, *65*, 2249.
(12) Gutman, A.; Penner, S. S. *J. Chem. Phys.* **1962**, *36*, 98.
(13) Vosper, A. J. *J. Chem. Soc. A* **1970**, *1*, 625.
(14) Koput, J.; Seibert, J. W. G.; Winnewisser, B. P. *Chem. Phys. Lett.* **1993**, *204*, 183.
(15) Fateley, W. G.; Bent, H. A.; Crawford, B. *J. Chem. Phys.* **1959**, *31*, 204.
(16) Hisatsune, I. C.; Devlin, J. P.; Wada, Y. *J. Chem. Phys.* **1960**, *33*, 714.
(17) Varetti, E. L.; Pimentel, G. C. *J. Chem. Phys.* **1971**, *55*, 3813.
(18) Givan, A.; Loewenschuss, A. *J. Chem. Phys.* **1989**, *90*, 6135.
(19) Givan, A.; Loewenschuss, A. *J. Chem. Phys.* **1989**, *91*, 5126.
(20) Givan, A.; Loewenschuss, A. *J. Chem. Phys.* **1991**, *94*, 7562.
(21) Pinnick, D. A.; Agnew, S. F.; Swanson, B. I. *J. Phys. Chem.* **1992**, *96*, 7092.
(22) Forney, D.; Thompson, W. E.; Jacox, M. E. *J. Chem. Phys.* **1993**, *99*, 7393.
(23) Wang, J.; Voss, M. R.; Busse, H.; Koel, B. E. *J. Phys. Chem. B* **1998**, *102*, 4693.
(24) Wang, J.; Koel, B. E. *J. Phys. Chem. A* **1998**, *102*, 8573.
(25) Wang, J.; Koel, B. E. *Surf. Sci.* **1999**, *436*, 15.
(26) Finlayson-Pitts, B. J.; Wingen, L. M.; Summer, A. L.; Syomin, D.; Ramazan, K. A. *Phys. Chem. Chem. Phys.* **2003**, *5*, 223.
(27) Ramazan, K. A.; Syomin, D.; Finlayson-Pitts, B. J. *Phys. Chem. Chem. Phys.* **2004**, *6*, 3836.
(28) Ramazan, K. A; Wingen, L. M.; Miller, Y.; Chaban, G. M.; Gerber, R. B.; Xantheas, S. S.; Finlayson-Pitts, B. J. *J. Phys. Chem. A* **2006**, *110*, 6886.

(29) Kleffmann, J.; Becker, K. H.; Wiesen, P. *J. Chem. Soc. Faraday Trans*. **1998**, *94*, 3289.
(30) Gerecke, A.; Thielmann, A.; Gutzwiller, L.; Rossi, M. J. *Geophys. Res. Lett.* **1998**, *25*, 2453.
(31) Kleffmann, J.; Becker, K. H.; Lackhoff, M.; Wiesen, P. *Phys. Chem. Chem. Phys.* **1999**, *1*, 5443.
(32) Kirchner, U.; Scheer, V.; Vogt, R. *J. Phys. Chem. A* **2000**, *104*, 8908.
(33) Borensen, C.; Kirchner, U.; Scheer, V.; Vogt, R.; Zellner, R. *J. Phys. Chem. A* **2000**, *104*, 5036.
(34) Parts, L.; Miller, J. T. *J. Chem. Phys.* **1965**, *43*, 136.
(35) Boldman, F.; Jodl, H. J. *Chem. Phys. Lett.* **1982**, *85*, 283.
(36) Agnew, S. F.; Swanson, B. I.; Jones, L. H.; Mills, R. L.; Schiferl, D. *J. Phys. Chem.* **1983**, *87*, 5065.
(37) Jones, L. H.; Swanson, B. I.; Agnew, S. F. *J. Chem. Phys.* **1985**, *82*, 4389.
(38) Rieley, H.; McMurray, D. P.; Haq, S. *J. Chem. Soc., Faraday Trans.* **1996**, *92*, 933.
(39) Sato, S.; Yamaguchi, D.; Nakagawa, K.; Inoue, Y.; Yabushita, A.; Kawasaki, M. *Langmuir* **2000**, *16*, 9533.
(40) Barney, W. S.; Finlayson-Pitts, B. J. *J. Phys. Chem. A* **2000**, *104*, 171.
(41) Yabushita, A.; Inoue, Y.; Senga, T.; Kawasaki, M.; Sato, S. *J. Phys. Chem. A* **2004**, *108*, 438.
(42) Harrar, J. E.; Rigdon, L. P.; Rice, S. F. *J. Raman Spectrosc.* **1997**, *28*, 891.
(43) Stirling, A.; Papai, I.; Mink, J.; Salahub, D. R. *J. Chem. Phys.* **1994**, *100*, 2910.
(44) Wang, X. F.; Qin, Q. Z.; Fan, K. N. *J. Mol. Struct.* **1998**, *432*, 55.
(45) Hohenberg, P.; Kohn, W. *Phys. Rev.* **1964**, *136*, B864.
(46) Kohn, W.; Sham, L. J. *Phys. Rev.* **1965**, *140*, A1133.
(47) Parr, R. G.; Yang, W. *Density-Functional Theory of Atoms and Molecules*; Oxford University Press: Oxford, 1989.
(48) Frisch, M. J.; Trucks, G. W.; Schlegel, H. B.; Scuseria, G. E.; Robb, M. A.; Cheeseman, J. R.; Montgomery, J. A., Jr.; Vreven, T.; Kudin, K. N.; Burant, J. C.; Millam, J. M.; Iyengar, S. S.; Tomasi, J.; Barone, V.; Mennucci, B.; Cossi, M.; Scalmani, G.; Rega, N.; Petersson, G. A.; Nakatsuji, H.; Hada, M.; Ehara, M.; Toyota, K.; Fukuda, R.; Hasegawa, J.; Ishida, M.; Nakajima, T.; Honda, Y.; Kitao, O.; Nakai, H.; Klene, M.; Li, X.; Knox, J. E.; Hratchian, H. P.; Cross, J. B.; Adamo, C.; Jaramillo, J.; Gomperts, R.; Stratmann, R. E.; Yazyev, O.; Austin, A. J.; Cammi, R.; Pomelli, C.; Ochterski, J. W.; Ayala, P. Y.; Morokuma, K.; Voth, G. A.; Salvador, P.; Dannenberg, J. J.; Zakrzewski, V. G.; Dapprich, S.; Daniels, A. D.; Strain, M. C.; Farkas, O.; Malick, D. K.; Rabuck, A. D.; Raghavachari, K.; Foresman, J. B.; Ortiz, J. V.; Cui, Q.; Baboul, A. G.; Clifford, S.; Cioslowski, J.; Stefanov, B. B.; Liu, G.; Liashenko, A.; Piskorz, P.; Komaromi, I.; Martin, R. L.; Fox, D. J.; Keith, T.; Al-Laham, M. A.; Peng, C. Y.; Nanayakkara, A.; Challacombe, M.; Gill, P. M. W.; Johnson, B.; Chen, W.; Wong, M. W.; Gonzalez, C.; Pople, J. A. *Gaussian 03*, Revision A.1; Gaussian, Inc.: Pittsburgh PA, 2003.
(49) Becke, A. D. *J. Chem. Phys.* **1993**, *98*, 5648.
(50) Lee, C.; Yang, W.; Parr, R. G. *Phys. Rev. B* **1988**, *37*, 785.
(51) Miehlich, B.; Savin, A.; Stoll, H.; Preuss, H. *Chem. Phys. Lett.* **1989**, *157*, 200.
(52) Vosko, S. H.; Wilk, L.; Nusair, M. *Can. J. Phys*. **1980**, *58*, 1200.
(53) Perdew, J. P. *Phys. Rev. B* **1986**, *33*, 8822.
(54) Perdew, J. P.; Burke, K.; Wang, Y. *Phys. Rev. B* **1996**, *54*, 16533.
(55) Becke, A. D. *J. Chem. Phys.* **1996**, *104*, 1040.
(56) Adamo, C.; Barone, V. *J. Chem. Phys.* **1998**, *108*, 664.
(57) Perdew, J. P.; Burke, K.; Ernzerhof, M. *Phys. Rev. Lett.* **1996**, *77*, 3865.
(58) Perdew, J. P.; Burke, K.; Ernzerhof, M. *Phys. Rev. Lett*. **1997**, *78*, 1396.
(59) Barbosa, R. C.; da Silva, A. B. F. *Mol. Phys.* **2003**, *101*, 1073.
(60) Peng, C.; Ayala, P. Y.; Schlegel, H. B.; Frisch, M. J. *J. Comput. Chem.* **1996**, *17*, 49.
(61) Cossi, M.; Scalmani, G.; Rega, N.; Barone, V. *J. Chem. Phys.* **2002**, *117*, 43.
(62) Fueno, T. *The Transition State. A Theoretical Approach*; Gordon and Breach Science Publishers: Amsterdam, 1999.
(63) Bilbart, C. H.; Ewing, G. E. *J. Chem. Phys.* **1974**, *61*, 1284.
(64) Melen, F.; Pokorni, F.; Herman, M. *Chem. Phys. Lett.* **1992**, *194*, 181.
(65) Smith, G. R.; Guillory, W. A. *J. Mol. Spec.* **1977**, *68*, 223.
(66) Harcourt, R. D.; Wolynec, P. P. *J. Phys. Chem. A* **2000**, *104*, 2138.
(67) Ornellas, F. R.; Resende, S. M.; Machado, F. B. C.; Roberto-Neto, O. *J. Chem. Phys.* **2003**, *118*, 4060.
(68) Wesolowski, S. S.; Fermann, J. T.; Crawford, T. D.; Schaefer, H. F. *J. Chem. Phys.* **1997**, *106*, 7178.
(69) Koput, J. *Chem. Phys. Lett.* **1995**, *240*, 553.
(70) Seidl, M. *Int. J. Quantum Chem.* **2003**, *91*, 145.
(71) Elyoussoufi, Y.; Herman, M.; Lievin, J.; Kleiner, I. *Spectrochim. Acta A* **1997**, *53*, 881.
(72) Bandow, H.; Akimoto, H.; Akiyama, S.; Tezuka, T. *Chem. Phys. Lett.* **1984**, *111*, 496.
(73) Song, Y.; Hemley, R. J.; Liu, Z.; Somayazulu, M.; Mao, H. K.; Herschbach, D. R. *J. Chem. Phys.* **2003**, *119*, 2232.
(74) Chou, A.; Li, Z.; Tao, F. M. *J. Phys. Chem. A* **1999**, *103*, 7848.